Experimental and Numerical Study of Rotor Aeroacoustics

Robert Stepanov[1], Vladimir Pakhov[2], Andrey Bozhenko[3], Andrey Batrakov[4], Lyaysan Garipova[5], Alexander Kusyumov[6], Sergey Mikhailov[7],
Kazan National Research Technical University n.a. A.N. Tupolev (*KAI*)*, 10 Karl Marx St., Kazan, 420111, Russian Federation*
and
George N. Barakos[8]
University of Glasgow, School of Engineering, Glasgow G12 8QQ, UK.

Abstract
The work documents recent experiments at the Kazan National Research Technical University named after A.N. Tupolev (KNRTU-KAI), related to helicopter acoustics. The objective is to measure near-field acoustics of rotors in hover and provide data suitable for CFD validation. The obtained set of data corresponds to a Mach-scaled rotor of known planform and the results are of high resolution. An advantage of the current dataset is that direct near-field acoustic data is made available and this allows for easy and direct comparisons with CFD predictions, without the need to use far-field aeroacoustic methods.

Nomenclature

Latin

r	=	horizontal distance from the rotor's axis of rotation
y	=	vertical distance from the rotor plane. Positive in the upstream direction
R	=	rotor radius ($R = 0.820\ m$)
$\bar{r}$	=	relative horizontal distance, scaled to the rotor radius R ($\bar{r} = r/R$)
$\bar{y}$	=	relative vertical distance, scaled to the rotor radius R ($\bar{y} = y/R$)
$\theta_{.75}$	=	collective pitch angle at 75% radius

Acronyms

KNRTU-KAI	=	Kazan National Research Technical University named after A.N. Tupolev (Kazan Aviation Institute)
SPL	=	Sound Pressure Level
WT	=	Wind Tunnel

1. Introduction

Improvement of helicopter performance has always been the objective of helicopter design engineers. However, while helicopter aerodynamic efficiency is of paramount importance during

[1]Junior Researcher, Department of Aerohydrodynamics; rpstepanov@kai.ru
[2]Junior Researcher, Department of Aerohydrodynamics; pahov.agd@kstu-kai.ru
[3]Junior Researcher, Department of Aerohydrodynamics; anbozhenko@kstu-kai.ru
[4]Junior Researcher, Department of Aerohydrodynamics; batrakov_a.c@mail.ru
[5]Junior Researcher, Department of Aerohydrodynamics; lyaysan_garipova@mail.ru
[6] Professor, Department of Aerohydrodynamics; ANKusyumov@kai.ru
[7] Professor, Department of Aerohydrodynamics; sergey.mikhaylov@kai.ru
[8] Professor, School of Engineering, James Watt South Bld., school of Engineering, University of Glasgow; george.barakos@glasgow.ac.uk. RAeS Member, corresponding author.

the helicopter design phase, satisfying the ever-growing low aeroacoustic emission requirements of aircraft has become very important in recent years. Nowadays, design engineers must comply with the stringiest noise regulations for new rotorcraft designs to be allowed to operate in airports and densely populated areas.

In recent years, research on aeroacoustic noise reduction of rotorcraft has been gaining momentum. Due to the fact that rotor blades are the main contributors to helicopter noise, most recent research efforts have been focused on analyzing acoustic noise of rotors [1-8]. The complexity of anaeroacoustic experiments is determined by the high cost of helicopter rig designs and the requirement to carry out the experiments in specially equipped low noise wind tunnels. Data of aeroacoustic rotor experiments are widely used by the CFD community to validate simulation results.

Rotor noise contains broadband and discrete noise components, which are all perceived by an observer. However, these components can be considered separately during mathematical modeling, where the discrete-frequency noise is divided into deterministic components of thickness, loading and high-speed impulsive noise tones that are dominant throughout the flight envelope of the helicopter [9]. The broadband noise includes non-deterministic loading noise, which includes blade self-noise, blade wake interaction noise and turbulent ingestion noise.

Thickness noise occurs because of the displacement of the air by the blade. It is mainly determined by the aerofoil thickness and rotor speed. It propagates mainly in the rotor plane in front of the upcoming blade. This type of noise occurs mostly at the tip of the rotor due to high tangential speeds of the blade sections. The thickness noise is the dominant noise component for an observer on the rotor plane, especially for hovering rotors.

Loading noise occurs as a result of fluid acceleration caused by a passing blade and it is directed primarily below the rotor. Minimization of the loading noise is important because it is usually considered as one of main noise sources of rotors [9].

The experience gained from the HART program [10-12] has shown that the key parameter for noise simulation is the successful wake simulation especially if BVI noise is considered. To this end, prescribed wake theory [13] and free wake simulation [10,14,15] have been successfully used in the past.

In a separate study [16], the pressure field near a small scale rotor blade was investigated at the University of Texas (USA), with a number of microphones arranged in a circular fashion about the tip of the rotor blade. In addition, measurements of the flow field near the blade tip were performed to identify flow structures inherent to the rotor.A comprehensive review of the rotor blade tip design technology was made by Brocklehurst and Barakos [17].

Most of well known open source references are dedicated to experiments with a far-field observer, located at a distance of several main rotor radii. In those conditions, the problem of aerocacoustic emission can be solved in two steps. During the first stage, flow parameters in the vicinity of the helicopter rotor blade can be evaluated with the CFD simulations. During the second stage, the data is used to set up an augmented mathematical model of the aeroacoustic wave propagation, based on different approaches: Ffowcs Williams – Hawkings [18] or Kirchhoff [19] equations, Curle's analogy [20], etc.

Obtaining the near-field aeroacoustic characteristics of the rotor with CFD simulation does not require any additional mathematical model (like the Kirchhoff equation). The near-field aeroacoustic flow parameters can be determined based on the results of CFD simulations, and more specifically, from the flow parameters near the blade surface. However, in this case it is crucial to have reliable experimental data for validation of CFD results.

This work presents experimental measurements of near-field pressure fluctuation in temporal domain of a main rotor model in hover, which can then be used by CFD community for validation of simulation results. The experimental results were obtained using the helicopter rotor rig of the T-1K wind tunnel of KNRTU-KAI. Experimental near-field data are then compared to CFD simulations results, obtained using the in-house HMB code. Some results of using the HMB solver for a far-field observer were previously presented in [21].

At the moment, the access to all experimental data of near-field aeroacoustic measurements is limited. However, all data, presented in this paper, will be made publicly available in the future, including the blade shape geometry and data of all measurements [22].

2. Experimental setup and experimental conditions

2.1. Wind tunnel

The current experiments were conducted in the acoustic chamber of the T-1K wind tunnel (WT) at KNRTU-KAI (Kazan, Russia), which is a single return, closed-circuit, open-jet WT with a contraction ratio of 4.9. The WT can be operated at wind speeds up to 50 m/s and it has a free-stream turbulence intensity below 0.5% in the jet core and a nozzle exit diameter of 2.25 m. To perform the acoustic and aerodynamic experiments, modifications were necessary, including the addition of ceiling and side walls, running between the jet and diffuser. The walls can be lifted or lowered in situ, as shown in Figure 1. It should be noted, however, that all the results presented in this work, were obtained for both walls at the lowered configuration. A schematic of the wind tunnel without the anechoic side walls is shown in Figure 2.

The retractable walls include Helmholtz resonators for absorbing acoustic noise of low frequencies coupled with pyramid shape melamine foam material for absorbing acoustic noise of higher frequencies. The Helmholtz resonators were designed to enable aero-acoustic rotor measurements of the rotor rig at lower frequencies (see Figure 2 for an overview of the test section).

Mach-scaled rotors have high rotational speeds, and tend to generate acoustic pressure in much higher frequencies compared to full size helicopters. Therefore, the acoustic absorbing material was selected to satisfy those requirements.

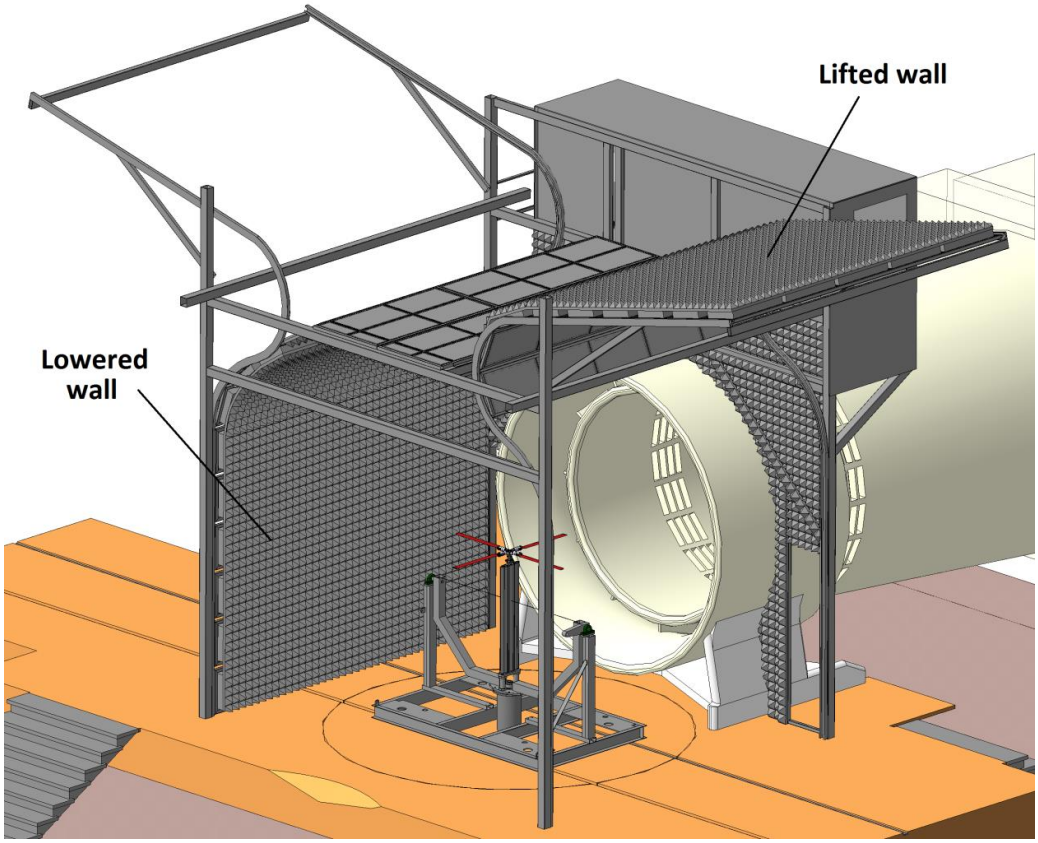

Figure 1. 3D model of the modified T-1K wind tunnel in KNRTU-KAI (Kazan, Russia). The side walls are shown in lowered and lifted configurations. The nozzle and adjacent to it walls are not shown for clarity.

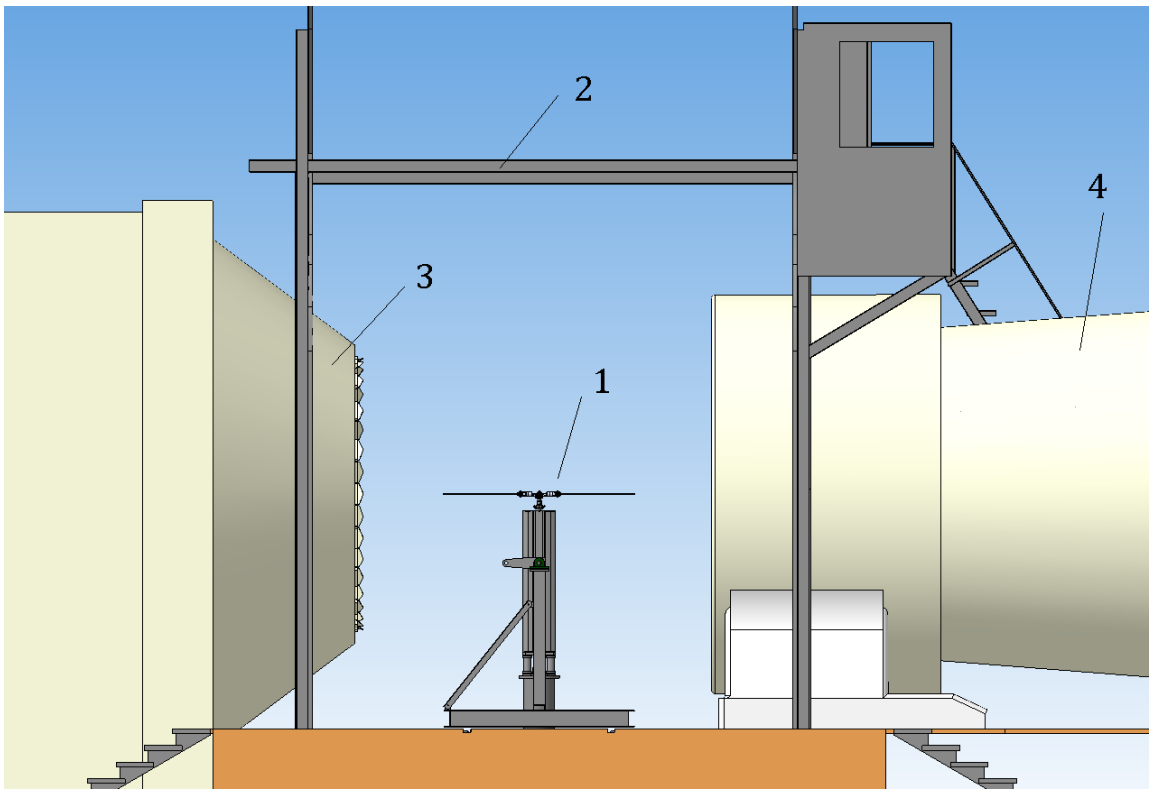

Figure 2. Schematic of the modified T-1K wind tunnel in KNRTU-KAI (Kazan, Russia). 1 – rotor rig; 2 – acoustic chamber; 3 – wind tunnel nozzle; 4 – wind tunnel diffuser.

2.2. Rotor rig

The rotor rig, used in this study, is presented in this section. A schematic of the rotor rig is shown in Figures 3 and 4.

The rotor rig could reach up to 2500 rpm of the rotational speed, its collective pitch could vary from -15° to +15° with an option of cyclic pitch control; the rotor shaft angle could vary from -30° to +30°. In this work, the angular speed was set to 900 rpm, which corresponded to the tip Mach number $M_{tip} = 0.23$. The collective pitch angle $\theta_{.75}$ was set to +8°. All tests were performed in hover mode, i.e. with no free stream velocity. The rotor radius was $R = 0.820\ m$, the blades had a constant chord of 65 mm along their span with rounded tips and no twist. The blade's airfoil had 0.5 percent camber and 14.9 percent thickness, as shown in Figure 5. In this work, all the distances are presented in terms of relative radius $\bar{r} = r/R = 1.2$, where r is a horizontal distance from the rotor's axis of rotation, and the relative distance $\bar{y} = y/R$, where y is a vertical distance from the rotor plane (see Figure 4).

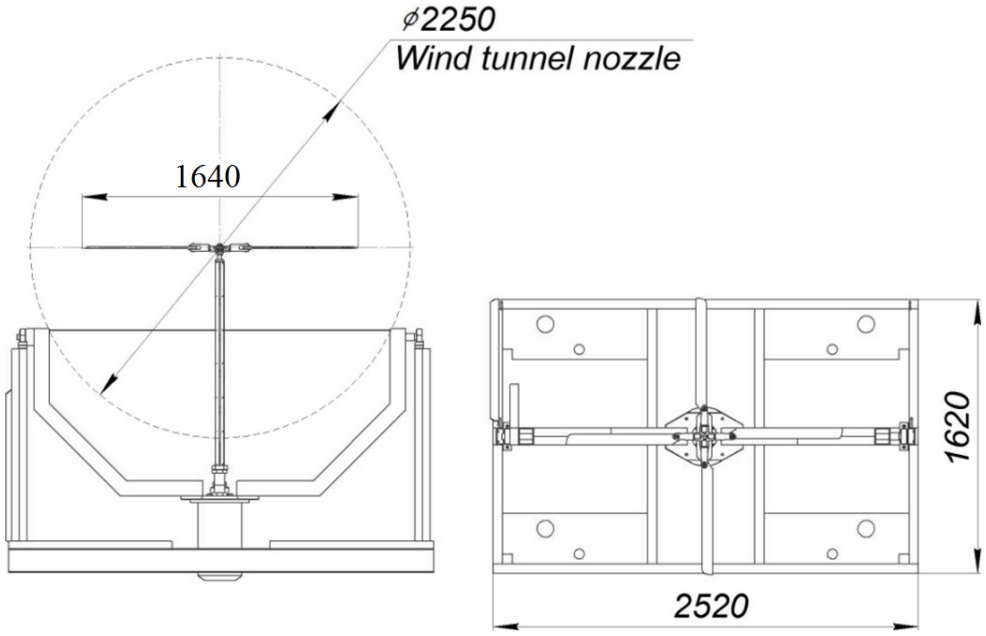

Figure 3. Rotor rig used in the T-1K wind tunnel. All dimensions in millimeters.

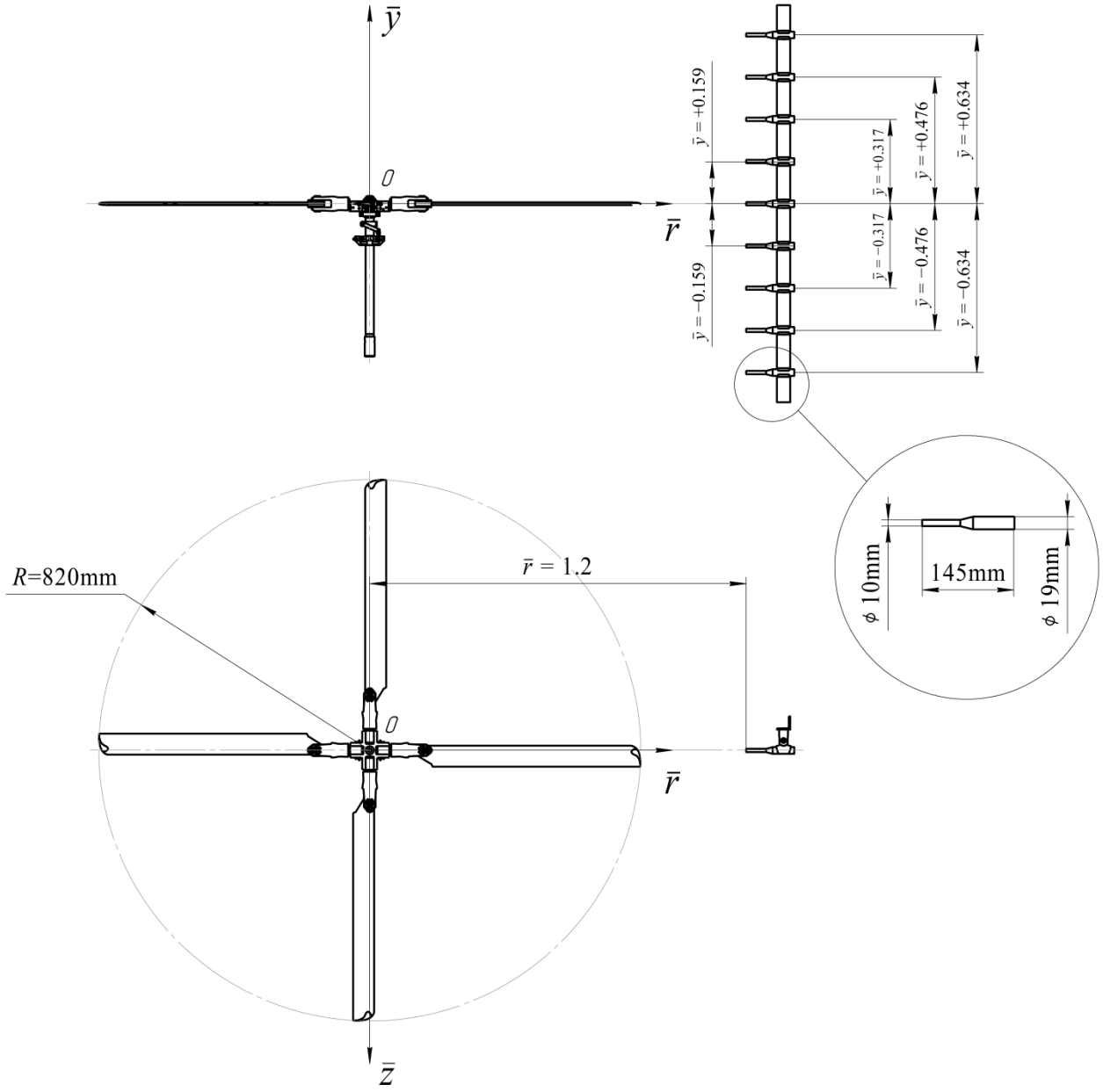

Figure 4. Microphone positioning during the experiments. The linear array is shown on the side view, and the distance from the array to the rotor is shown on the top view.

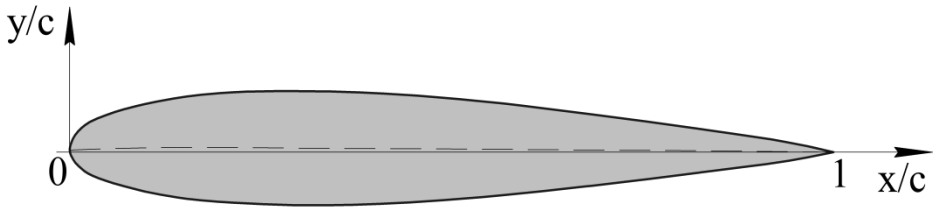

Figure 5. Airfoil of the rotor blade.

2.3. Data acquisition and analysis

The measurements were taken with DBX RTA-M microphones coupled with Panasonic WM-61A cartridges. An NI-PXI 4496 ADC card, supporting sampling rates of up to 204kS/s with 24-bit analogue-to-digital conversion, was used. For the measurements at hand, 9 out of 64 channels were

used, forming a linear array of 9 microphones, as shown in Figure 4. This setup allowed recording signals from 9 microphones simultaneously. The measurements were acquired over 10 seconds with a sampling rate of 48kHz.

The microphone placement along with the geometrical dimensions of the microphones are shown in Figure 4, with the microphone array positioned at a relative radius $\bar{r} = 1.2$.

Due to the periodicity of the signal with respect to the blade pass frequency, the pressure distribution in the temporal domain was statistically analyzed.

The phase-averaged signal p_{avg} was estimated using the following equation:

$$p_{avg} = \frac{1}{N}\sum_{i=1}^{N} p_{ij}.$$

Here i is the number of the period, which corresponds to the time frame of one passing blade, and j is the phase position of the pressure reading p_{ij} along that period.

The confidence intervals corresponded to $\pm\sigma_j$, where σ_j is the root-mean-square deviation:

$$\sigma_j = \sqrt{\frac{1}{N}\sum_{i=1}^{N}(p_{avg} - p_{ij})^2}.$$

3. CFD setup and conditions

Numerical simulations of the flow around the model rotor in hover were based on the RANS approach with the k-ω turbulence model, and carried out with HMB CFD-code [20]. The flow around the isolated rotor in hover mode has a periodic structure. For this reason, a computational domain was constructed for one blade only (see Figure 6). A multiblock grid was created using the ICEM Hexa™ tool and contained 4.4 million points. The wake topology, obtained from CFD computations, is shown in Figure 7.

The near field sound generation at any considered point is determined by the fluctuation of static pressure due to the rotation of the rotor. The grid consisted of 172 blocks and 4.4 millions of points with a careful arrangement to capture the loading of the blade and provide good resolution of the wake. The grid was constructed using previous experience with similar configurations [23], and while it is coarse, it captures the main flow features with relatively good accuracy.

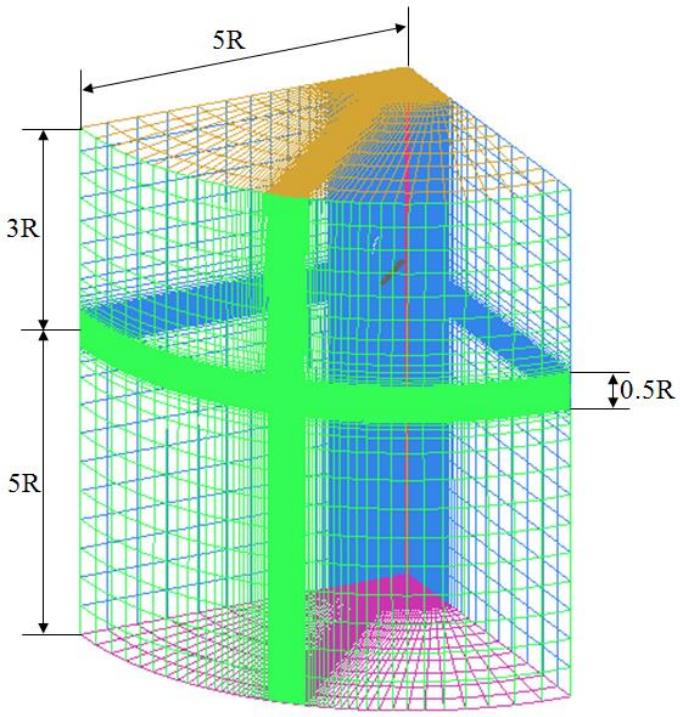

Figure 6. Computational grid for one blade of the rotor.

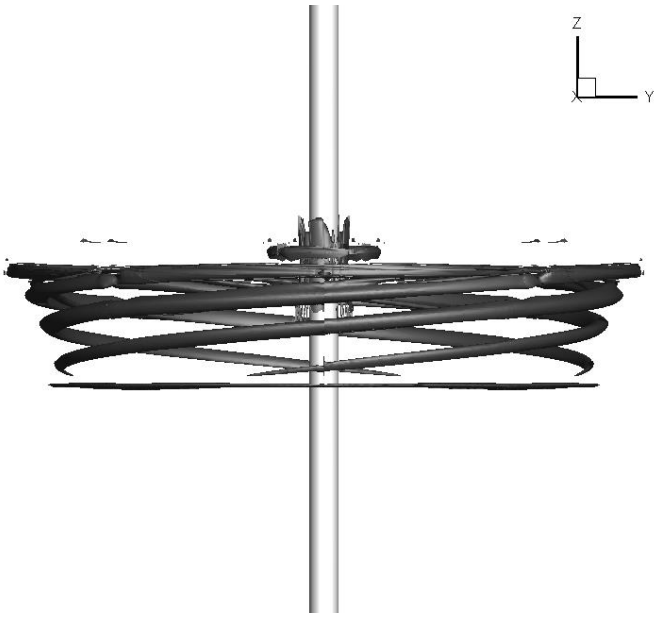

Figure 7. Wake topology obtained from CFD computations.

4. Results and Discussion

The linear array was placed at the relative distance $\bar{r}$ =1.2 from the rotor plane. In order to estimate possible influence of the microphone array on the flow field, the scaled microphone contours were added next to the speed distribution, obtained from CFD computations of the isolated rotor, in the vicinity of the rotor plane (see Figure 8). It can be seen, that the speed values of the flow field are very low in the vicinity of the microphone array.

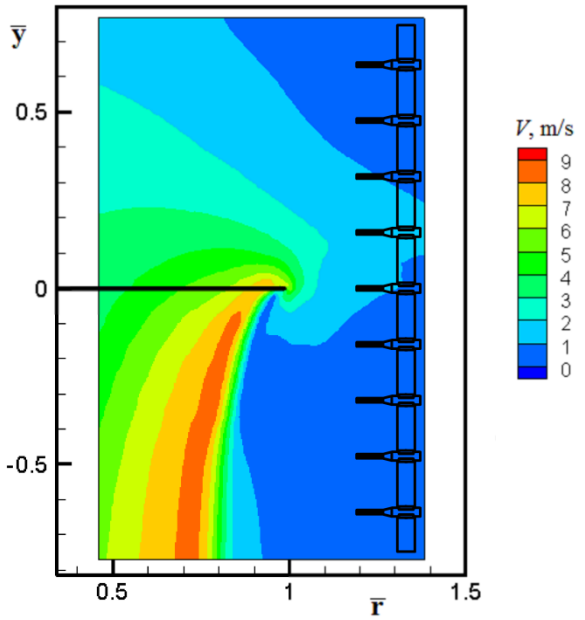

Figure 8. The speed distribution around the rotor plane, obtained from CFD computations, and the linear microphone array.

Comparison of sound pressure levels (SPL) in the temporal domain for experimental results and CFD computations are shown in Figures 9-17. The experimental data was phase averaged, as described earlier. The phase-average pressure distribution along with their corresponding confidence intervals are compared to the results of the CFD computations. The time span in those figures corresponds to the period of a passing blade, i.e. to one quarter of a revolution.

Figures 9-17 show that the peaks of the acoustic pressure levels occur slightly upstream of the rotor plane and are much less pronounced at the same distances downstream of the rotor. The comparison of the experimental and CFD data also show that these results are in good agreement with each other.

The difference of the noise signatures observed in Figures 11-13 can be attributed to factors, such as the coning angle of the rotor and the test section boundaries. The coning changed depending on the operating conditions of the rotor during the experiments, but was set to zero for the CFD computations because the simulations were carried out blindly before the experiment. The CFD modeling also assumes the rotor operating in an infinite domain. As for the experiment, the rotor was located inside of the acoustic chamber described in Section 2.1.

The comparison of SPL levels between the experimental data and CFD computations is shown in Figure 18. The SPL levels are presented in terms of peak-to-peak decibel values of the signal. The comparison of experiment and CFD computations for the linear microphone array is shown on the left-hand side of Figure 18, which was obtained from Figures 9-17. The directivity diagram of the acoustic SPL in the near-field ($1.2R$) from CFD computations is shown on the right-hand side of Figure 18. One point from the experimental results is also added to the diagram, which shows a good agreement with CFD results. It can also be seen that the sound pressure peaks occur slightly above the rotor plane.

The collective pitch angle for this simulation was also set to 8 degrees, and the blade coning angle was equal to zero. However, the coning angle was not a constant value during the experiment, and it changed depending on different operational conditions of the rotor.

Figure 19 presents experimental and CFD results of wake boundaries in hover flight obtained in KNRTU-KAI [24]. The flow visualization was performed using a Dantec PIV system with an Nd:YAG laser. The vortices were identified using Q-criterion for a 2D case, defined as connected spatial regions, where the Euclidean norm of the vorticity tensor dominates the rate of the strain tensor, i.e. when the $Q > 0$ condition is satisfied [25].

One of the exposure frames,obtained during the experiment, is shown in Figure 19 (a), where four distinct tip vortices can be seen. The vortices are shown along with the velocity field and streamlines. The position of each vortex, obtained in the experiment for multiple frames, is shown by dots in Figure 19 (b), which are then approximated with a polynomial line. The CFD results are then added to Figure 19 (b), and are in good agreement with the experiment.

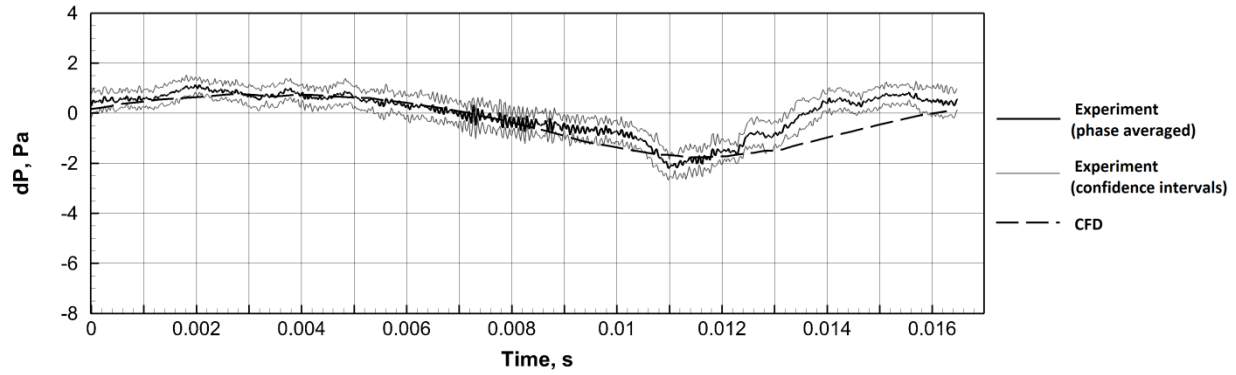

Figure 9. Comparison of the phase averaged pressure distribution with the corresponding confidence intervals to the CFD results. The vertical distance from the rotor plane to the microphone $\bar{y} = 0.634$.

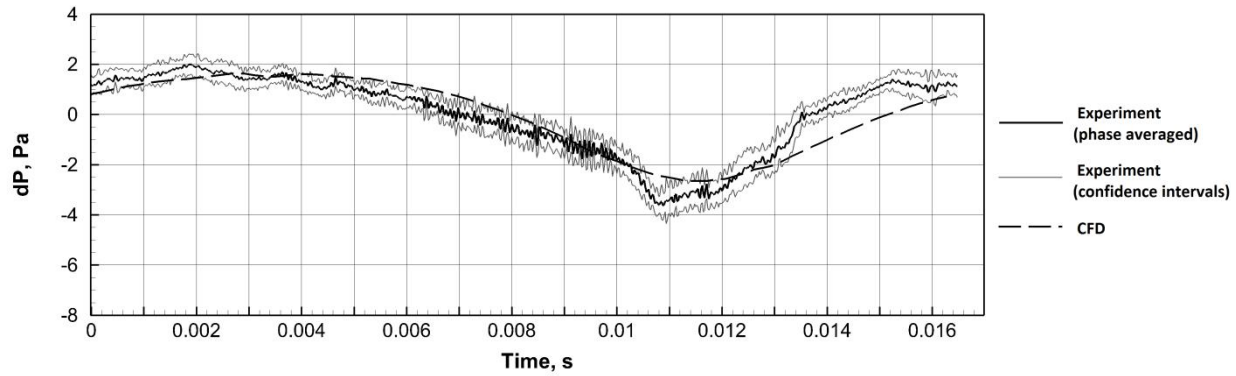

Figure 10. Comparison of the phase averaged pressure distribution with the corresponding confidence intervals to the CFD results. The vertical distance from the rotor plane to the microphone $\bar{y} = 0.476$.

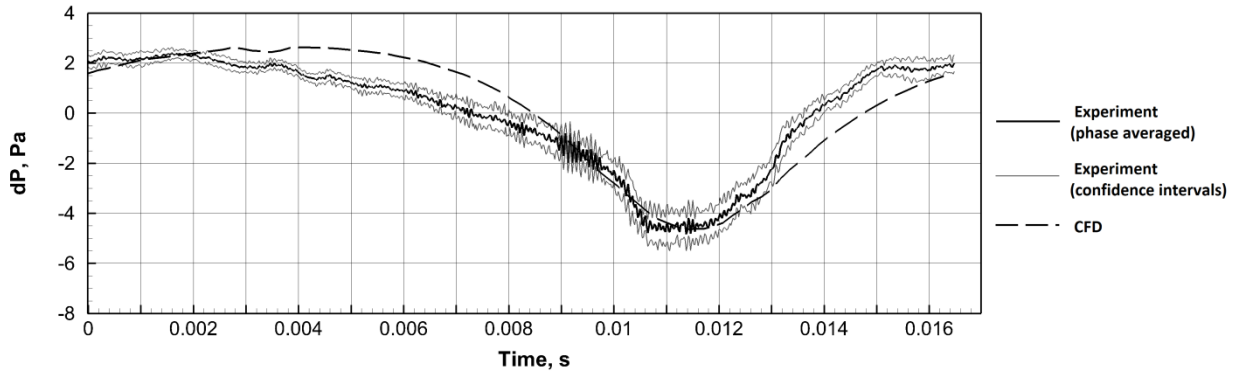

Figure 11. Comparison of the phase averaged pressure distribution with the corresponding confidence intervals to the CFD results. The vertical distance from the rotor plane to the microphone $\bar{y} = 0.317$.

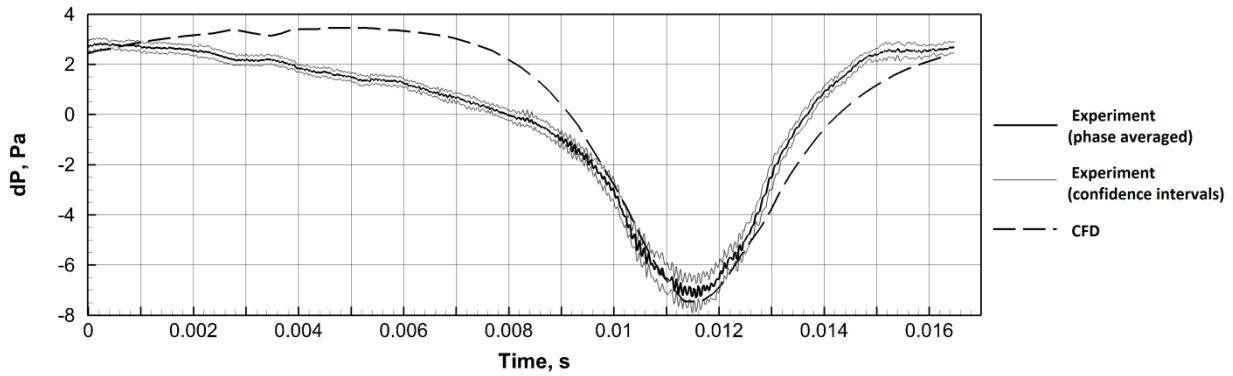

Figure 12. Comparison of the phase averaged pressure distribution with the corresponding confidence intervals to the CFD results. The vertical distance from the rotor plane to the microphone $\bar{y} = 0.159$.

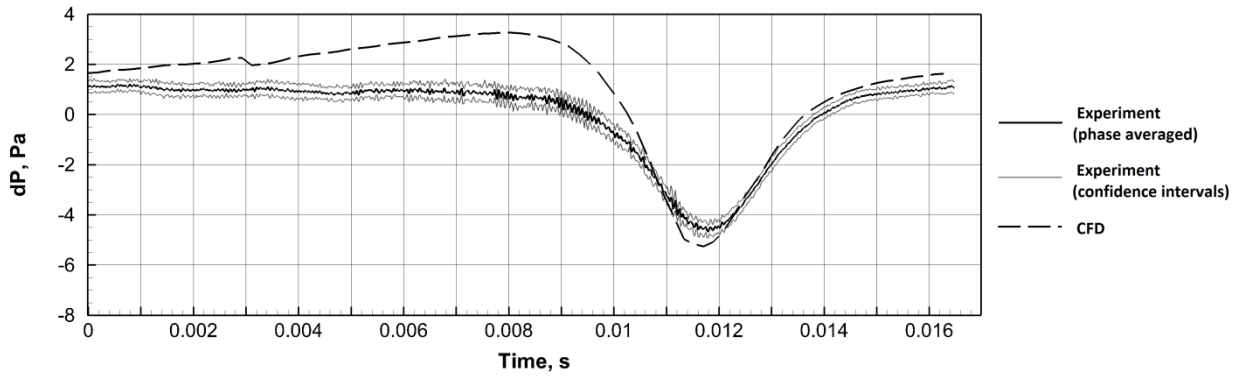

Figure 13. Comparison of the phase averaged pressure distribution with the corresponding confidence intervals to the CFD results. The vertical distance from the rotor plane to the microphone $\bar{y} = 0$.

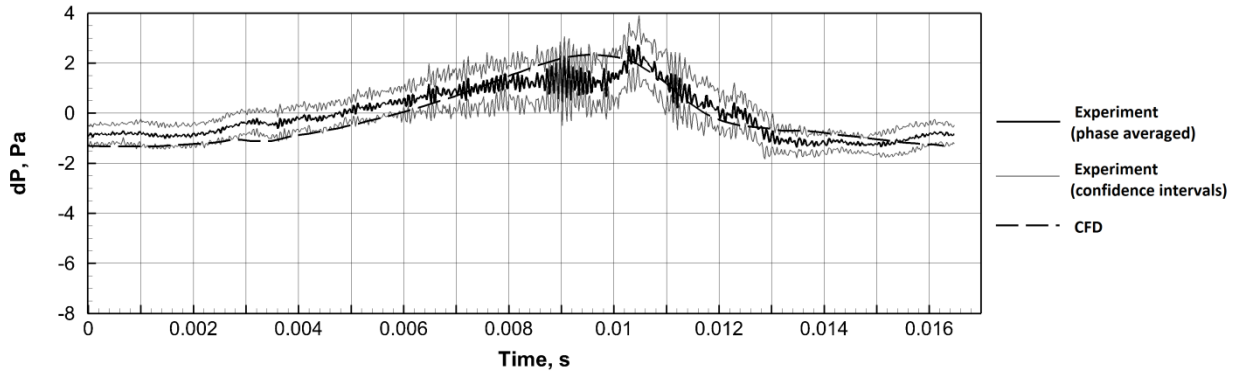

Figure 14. Comparison of the phase averaged pressure distribution with the corresponding confidence intervals to the CFD results. The vertical distance from the rotor plane to the microphone $\bar{y} = -0.159$.

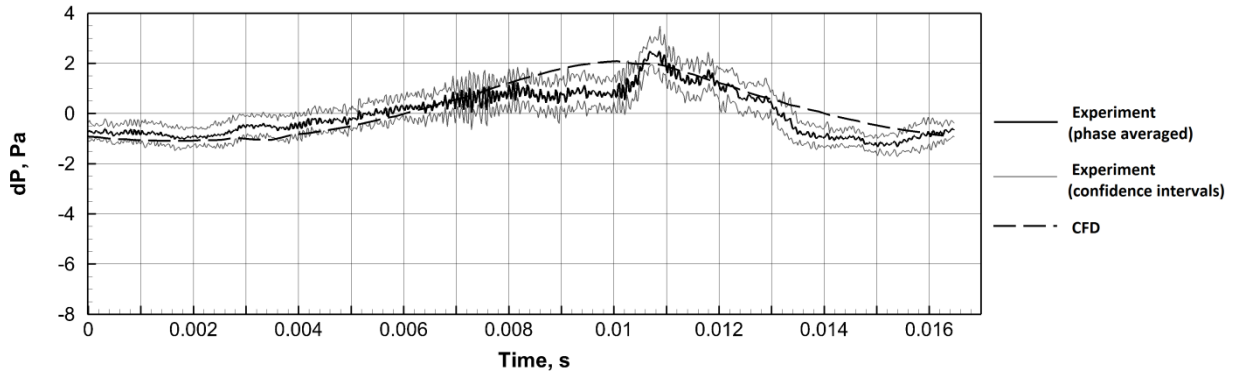

Figure 15. Comparison of the phase averaged pressure distribution with the corresponding confidence intervals to the CFD results. The vertical distance from the rotor plane to the microphone $\bar{y} = -0.317$.

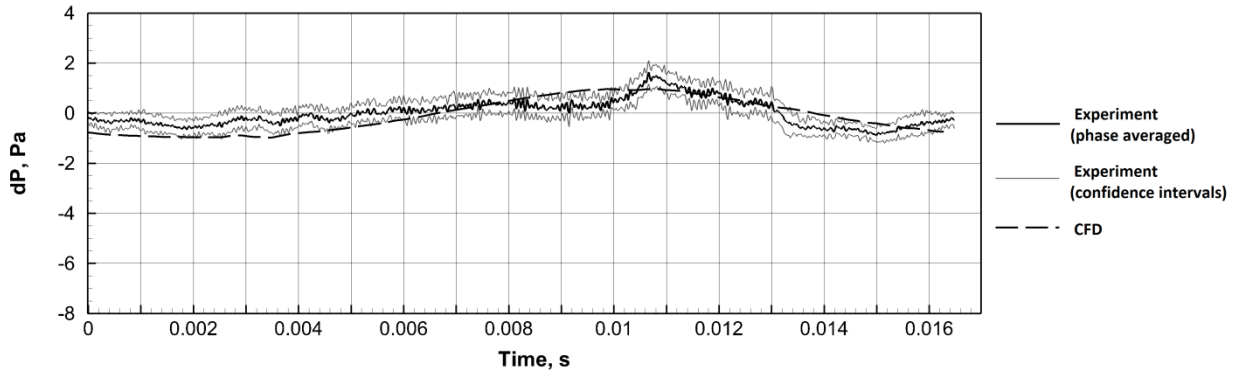

Figure 16. Comparison of the phase averaged pressure distribution with the corresponding confidence intervals to the CFD results. The vertical distance from the rotor plane to the microphone $\bar{y} = -0.476$.

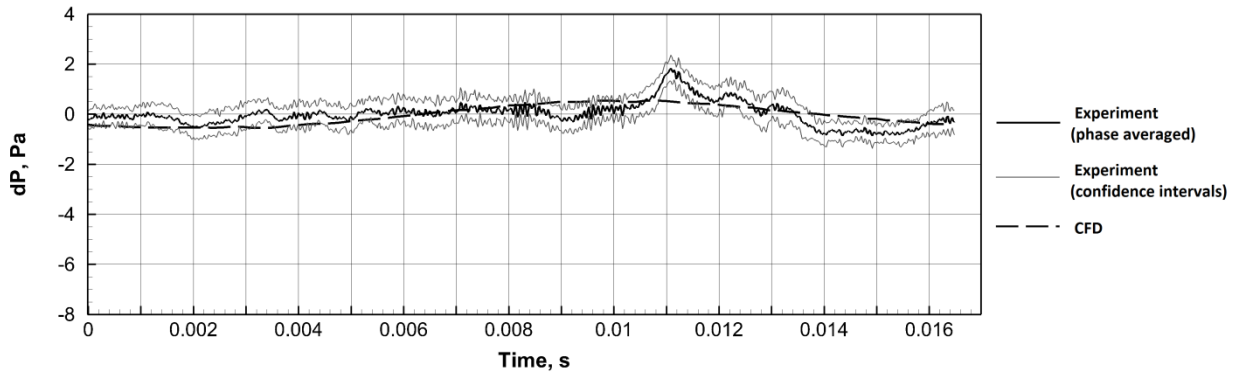

Figure 17. Comparison of the phase averaged pressure distribution with the corresponding confidence intervals to the CFD results. The vertical distance from the rotor plane to the microphone $\bar{y} = -0.634$.

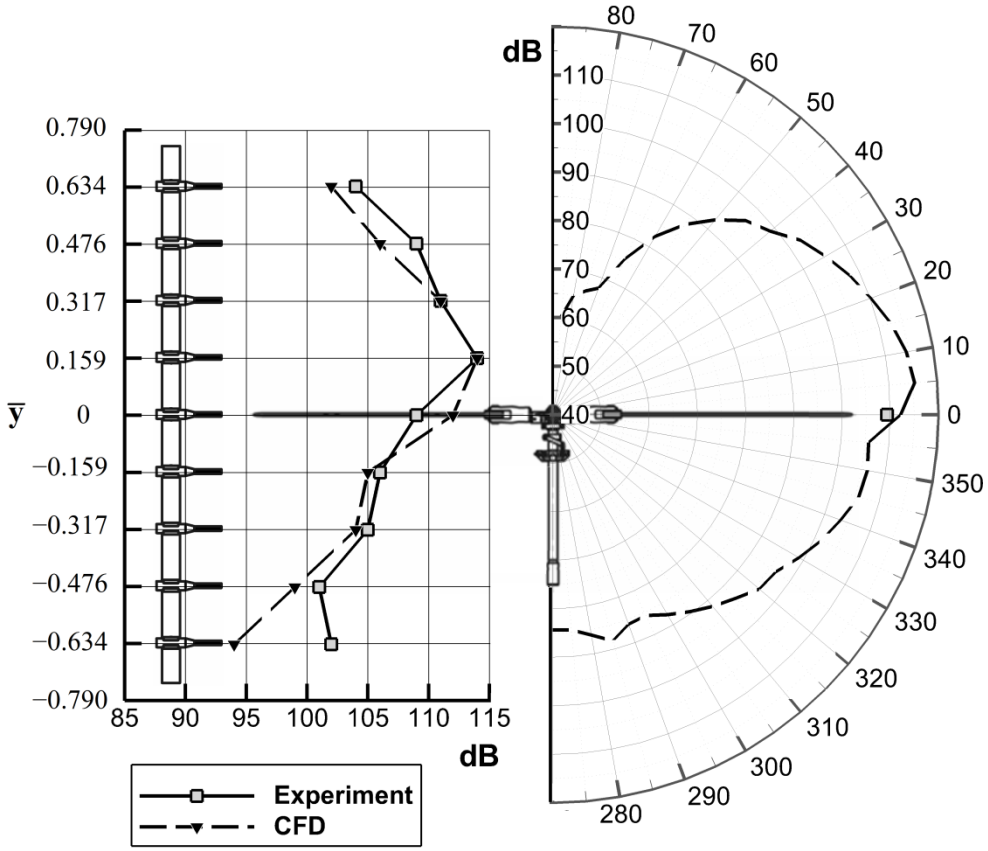

Figure 18. The comparison of SPL levels of the experiments with CFD computations: for the linear array at $\bar{r} = 1.2$ on the left-hand side, and for the directivity diagram at 1.2R on the right-hand side.

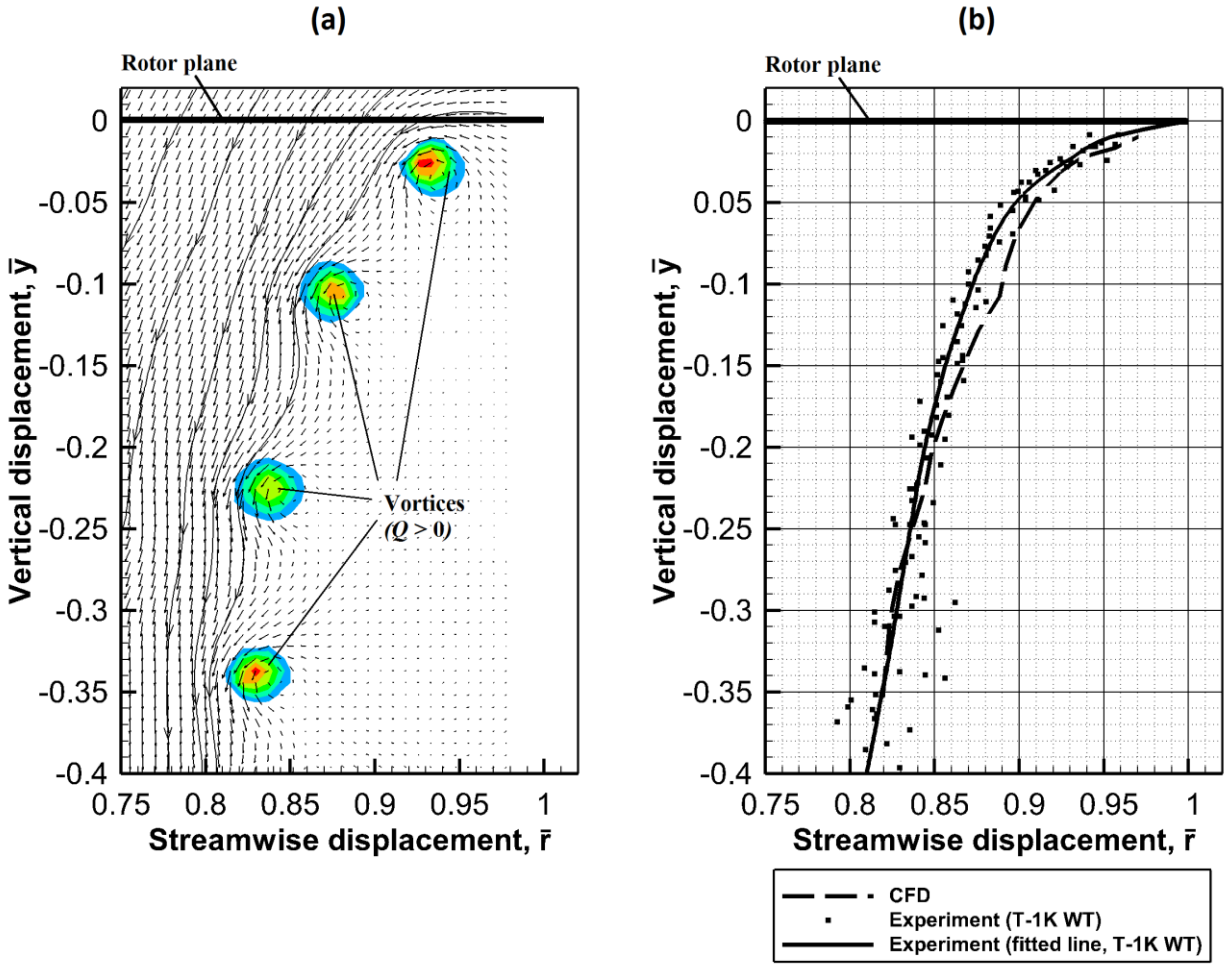

Figure 19. Comparison CFD with experimental results of tip vortex coordinates for hover ($C_T = 0.01$).

5. Conclusions and Future Work

The work presented experimental results obtained using a near-field linear array for a model-scale rotor in hover. The array consisted of 9 microphones and it was placed at $1.2R$ distance from the rotor. The comparison of experimental data with the CFD simulation results of acoustic pressure fluctuations in temporal domain showed good agreement. The CFD simulations were based on RANS solutions obtained using the in-house HMB code [26]. So far, the following conclusions can be drawn:

1. Experimental data can be used for initial validation of CFD solvers, which are easy to run and economic in CPU time.

2. The data appears to be accurate and agree with theoretical estimates and preliminary CFD-results.

Future studies will be aimed at forward flight with focus on BVI and HIS noise studies, using near-field microphone arrays. Future simulations are also to be performed for validating the HMB solver.

Acknowledgements

This work was supported by the grant 'Numerical and physical modelling of aerodynamic and aeroacoustic characteristics of rotor systems of future concept aircarft' (No. 9.1577.2017/ P Ch) of the Ministry of Education and Science of the Russian Federation.

References

1. Schmitz FH, Boxwell DA, Splettstoesser WR, Schultz KJ. Model-rotor high-speed impulsive noise: Full-scale comparisons and parametric variations. *Vertica*, 8(4), pp. 395-422, 1984.

2. van der Wall BG, Burley CL, Yu Y., Hugues R, Pengel K, Beaumier P. The HART II test – measurement of helicopter wakes.*Aerospace Science and Technology*. Volume 8, Issue 4, June 2004, pp.273-284.

3. Kube R, Splettstoesser WR, Wagner W, Seelhorst U, Yu YH, Tung C, Beaumier P., Prieur J, Rahier G, Spiegel P, Brooks TF, Burley CL, Boyd DD, Mercker E, Pengel K. HHC Aeroacoustic Rotor Tests in the German-Dutch Wind Tunnel: Improving Physical Understanding and Prediction Code. *Aerospace Science and Technology*, 1998, no. 3, 177-190.

4. Splettstoesser WR, Niesl G, Cedenese F, Nitti F, Papanikas D. Experimental Results of the European HELINOISE Aeroacoustic Rotor Test. *Journal of the American Helicopter Society*, Vol. 40, No. 2, 1995.

5. Schultz KJ, Splettstoesser WR, Junker B, Wagner W, Schoell E, Merker E, Pengel K, Arnaud G, Fertis D. A parametric Wind Tunnel Test on Rotorcraft Aerodynamics and Aeroacoustics (HELISHAPE) - Test Procedures and Representative Results. *22nd European Rotorcraft Forum*, September 1996, Brighton, UK, Paper No. 52.

6. Yu Y, Gmelin B, Heller H, Philippe J, Mercker E, Preisser J. HHC Aeroacoustic Rotor Test at the DNW - The joint German/French/US Project. Paper 115, *20th European Rotorcraft Forum*, October 1994, Amsterdam, Netherlands.

7. Heller H, Buchholz H, Schultz KJ, Ahmed SR, Splettstoesser WR. Helicopter Rotor Blade Aeroacoustics - A Comparison of Model-Scale Wind Tunnel and Full-Scale Flight Test Results. *20th ICAS Congress*, Sorrent, Italy, September 1996. Paper ICAS-96-1.8.1.

8. Harrison R, Stacey S, Hansford B. BERP IV the Design, Development and Testing of an Advanced Rotor Blade.*64th Annual Forum of the AHS*, Montreal, Canada, April 29-May 1, 2008.

9. Brentner KS, Farassat F. Modeling aerodynamically generated sound of helicopter rotors. *Progress in Aerospace Sciences*, 39, pp. 83 – 120, 2003.

10. van der WallBG, BurleyCL, YuY, Richard H, Pengel K, BeaumierP.The HART II test – measurement of helicopter wakes.*Aerospace Science and Technology*. Volume 8, Issue 4, June 2004, pp.273-284. (doi:10.1016/j.ast.2004.01.001).

11. Beaumier P, Spiegel P. Validation of ONERA prediction methods for blade-vortex interaction using HART results. *51st Annual Forum of the American Helicopter Society*, Fort Worth, TX, 1995.

12. van der WallBG. Vortex characteristics analysed from HART data. *23rd European Rotorcraft Forum*, Dresden, Germany, 1997.

13. van der WallBG. Simulation of HHC on helicopter rotor BVI noise emission using a prescribed wake method.*26th European Rotorcraft Forum*, The Hague, Netherlands, 2000.

14. Brooks TF, Boyd DD, Burley CL, JollyJR, Aeroelastic codes for rotor harmonic and BVI noise – CAMRAD.Mod1/HIRES.*2nd AIAA/CEAS Aeroacoustics Conference*, State College, PA, 1996.

15. van der WallBG, RothM. Free-wake analysis on massively parallel computers and validation with hart test data. *53rd Annual Forum of the American Helicopter Society*, Virginia Beach, VA, 1997

16. Stephenson JH, Tinney CE, Sirohi J. The near field pressure of a small-scale rotor during hover.*48th AIAA Aerospace Sciences Meeting Including the New Horizons Forum and Aerospace Exposition*, No. 01, 2010; DOI: 10.2514/6.2010-8.

17. Brocklehurst A, and Barakos GN. A Review of Helicopter Rotor Blade Tip Shapes. *Progress in Aerospace Sciences*, September, pp. 1-36, 2012. (dx.doi.org/10/1016/j.paerosci.2012.06.003)

18. Ffowcs Williams JE, Hawkings DL. Sound generated by turbulence and surfaces in arbitrary motion.*Philosophical Transactions of the Royal Society*, A264, 1969, pp. 321 – 342.

19. Brentner KS, FarassatF. An analytical comparison of the acoustic analogy and Kirchhoff formulation for moving surfaces.*AIAA Journal*, 36 (8), pp. 1379 – 86, 1998.

20. Curle N. The influence of solid boundaries upon aerodynamic sound.*Proc. Roy. Soc.A*, 231(1187), pp. 505–514, 1955.

21. Garipova LI, Batrakov AS, Kusyumov AN, Mikhailov SA, Barakos G. Aerodynamic and acoustic analysis of helicopter main rotor blade tips in hover. *International Journal of Numerical Methods for Heat & Fluid Flow*, Vol. 22, Iss: 5, pp. 554 – 575, 2016.

22. http://agd.kai.ru/

23. Garipova LI, Batrakov AS, Kusyumov AN, Mikhailov SA, Barakos G. Aerodynamic and acoustic analysis of main rotor blade tip part for hover. *International Journal of Numerical Methods for Heat & Fluid Flow*. Vol. 26, Issue 7, pp. 2101–2118.

24. Stepanov R, and Mikhailov S. Experimental investigation of main rotor wake. *MATEC Web of Conferences*, Vol. 115, 02013 (2017). (DOI: 10.1051/matecconf/201711502013).

25. Haller G. An objective definition of a vortex. *J. Fluid Mech.*, vol. 525, pp.1–26, 2005. (DOI: 10.1017/S0022112004002526).

26. Steijl R, and Barakos GN. Sliding mesh algorithm for CFD analysis of helicopter rotor–fuselage aerodynamics. *International Journal for Numerical Methods in Fluids*, Vol. 58, Issue 5, pp. 527–549.